Cell

Glucose Regulates Mitochondrial Motility via Milton Modification by *O*-GlcNAc Transferase

Gulcin Pekkurnaz,[1] Jonathan C. Trinidad,[2] Xinnan Wang,[3] Dong Kong,[4,5] and Thomas L. Schwarz[1,*]
[1]The F.M. Kirby Neurobiology Center, Boston Children's Hospital and Department of Neurobiology, Harvard Medical School, Boston, MA 02115, USA
[2]Department of Chemistry, Biological Mass Spectrometry Facility, Indiana University, Bloomington, IN 47405, USA
[3]Department of Neurosurgery, Stanford University, Stanford, CA 94304, USA
[4]Division of Endocrinology, Department of Medicine, Beth Israel Deaconess Medical Center, Harvard Medical School, Boston, MA 02215, USA
[5]Present address: Department of Neuroscience, Tufts University School of Medicine, Boston, MA 02116, USA
*Correspondence: thomas.schwarz@childrens.harvard.edu
http://dx.doi.org/10.1016/j.cell.2014.06.007

SUMMARY

Cells allocate substantial resources toward monitoring levels of nutrients that can be used for ATP generation by mitochondria. Among the many specialized cell types, neurons are particularly dependent on mitochondria due to their complex morphology and regional energy needs. Here, we report a molecular mechanism by which nutrient availability in the form of extracellular glucose and the enzyme *O*-GlcNAc Transferase (OGT), whose activity depends on glucose availability, regulates mitochondrial motility in neurons. Activation of OGT diminishes mitochondrial motility. We establish the mitochondrial motor-adaptor protein Milton as a required substrate for OGT to arrest mitochondrial motility by mapping and mutating the key *O*-GlcNAcylated serine residues. We find that the GlcNAcylation state of Milton is altered by extracellular glucose and that OGT alters mitochondrial motility in vivo. Our findings suggest that, by dynamically regulating Milton GlcNAcylation, OGT tailors mitochondrial dynamics in neurons based on nutrient availability.

INTRODUCTION

Mitochondria form a dynamic, interconnected network and play a vital role in cellular energetics by generating ATP, buffering calcium, and participating in metabolic pathways. Positioning mitochondria in areas of high-energy consumption followed by the induction of oxidative phosphorylation can allow cells to respond to increased energy demands. Therefore, the molecular mechanisms that relay signals to mitochondria about changes in local nutrient status and metabolic demand are critical for cell function (Liesa and Shirihai, 2013; Nunnari and Suomalainen, 2012).

Glucose is the predominant carbon source for ATP production by mitochondria. Neuronal metabolism in particular relies heavily on a continuous supply of glucose (Peppiatt and Attwell, 2004). Moreover, due to their elaborate morphology and regional differences in energy use and nutrient access, glucose uptake and handling are spatially heterogeneous in neurons (Ferreira et al., 2011; Hall et al., 2012; Weisová et al., 2009). Mitochondrial dynamics may therefore need to respond to changes in the glucose supply to ensure rapid ATP production, especially during intense synaptic activity and action potential firing.

The distribution of neuronal mitochondria is determined by the elaborate regulation of their motility (Chang et al., 2006). They can move in either direction, pause, change direction, or remain stationary. This behavior is primarily mediated by the interplay of (+)-end directed kinesin, (−)-end directed dynein motors, and anchoring proteins (Schwarz, 2013).

The mitochondrial motor/adaptor complex plays a central role in regulating this process (Wang and Schwarz, 2009b). The mitochondrial receptor for this complex, the GTPase Miro (also called RhoT1/2), interacts with the adaptor protein Milton (also called TRAK1/2 and OIP106/98), which couples kinesin heavy chain (KHC) and dynein/dynactin to mitochondria (Glater et al., 2006; Macaskill et al., 2009; van Spronsen et al., 2013). Milton also binds an enzyme called *O*-GlcNAc transferase (OGT) (Iyer et al., 2003; Iyer and Hart, 2003). OGT catalyzes the addition of a single sugar moiety onto serine and threonine residues of nuclear and cytoplasmic proteins, including Milton, in a process called *O*-GlcNAcylation. OGT has been considered a metabolic sensor for glucose (Hart et al., 2011) because *O*-GlcNAcylation levels are influenced by glucose flux via the hexosamine biosynthetic pathway (HBP), which produces the donor substrate, UDP-GlcNAc.

Although the OGT/Milton interaction is conserved from *Drosophila* (Glater et al., 2006) to mammals (Brickley et al., 2011; Iyer and Hart, 2003), its functional significance is unknown. We hypothesized that mitochondrial motility would be sensitive to glucose levels and that OGT-dependent Milton *O*-GlcNAcylation links glucose metabolism to the regulation of mitochondrial motility.

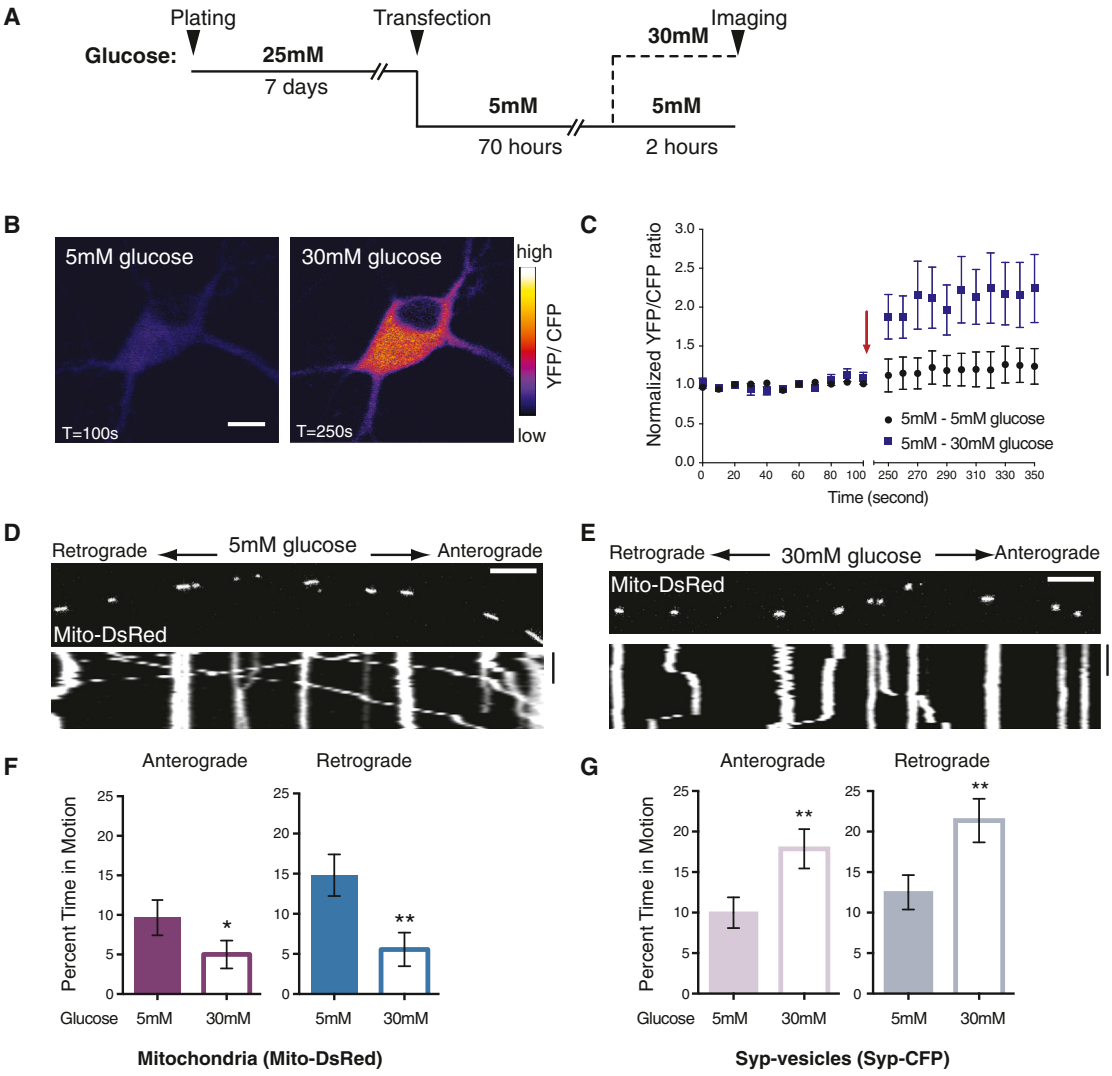

Figure 1. Increased Glucose Decreases Mitochondrial Motility in Rat Hippocampal Axons

(A) Schematic of the paradigm for changing extracellular glucose.

(B and C) The sensor FLII^{12}Pglu-600μδ6 was expressed in cultured rat hippocampal neurons and the YFP/CFP ratio used to determine intracellular glucose concentration in 5 mM and after switching to 30 mM glucose medium.

(B) Pseudocolored pixel-by-pixel ratio of a neuron before and after the switch to 30 mM glucose (scale bar, 10 μm).

(C) Normalized YFP/CFP ratios from neurons cultured in 5 mM glucose before and after exchange (arrow) of medium for either fresh 5 mM glucose (solid circle) or 30 mM glucose (solid square). 30 mM extracellular glucose caused ~2-fold increase in intracellular glucose ($p = 0.0007$, $n > 4$, three independent transfections).

(D and E) Representative kymographs of mitochondrial motility in hippocampal axons transfected with Mito-DsRed and synaptophysin (Syp)-CFP and imaged after culturing as schematized in (A). Here and in subsequent figures, the first frame of each time-lapse movie is shown above a kymograph generated from that region of axon. The y axis of each kymograph represents time, and the x axis depicts the position of the organelles such that stationary organelles appear as vertical lines, whereas those moving either anterograde or retrograde are diagonal. Scale bars, 10 μm and 100 s.

(F and G) The percent time each mitochondrion (F) or Syp vesicle (G) spent in anterograde and retrograde motion was calculated from kymographs like those in (D) and (E). $n = 73–101$ mitochondria from 8 axons, and $n = 114–126$ vesicles from 7 axons and 4 independent transfections per condition.

*$p < 0.05$ and **$p < 0.01$; Mann-Whitney *U* test. All values are shown as mean ± SEM. See also Movies S1, S2, S3, and S4 and Table S1.

RESULTS

Increased Extracellular Glucose Decreases Mitochondrial Motility in Hippocampal Axons

To examine the effects of elevated extracellular glucose on axonal mitochondrial motility, we performed live-cell imaging in rat hippocampal neurons expressing Mito-DsRed, a mitochondrial marker, and synaptophysin-CFP (Syp-CFP), a marker of synaptic vesicle precursors. Normal neurobasal (NB) medium contains a high level of glucose (25 mM), which likely saturates glucose transporters. Therefore, we switched established cultures to a preconditioning 5 mM glucose medium for 70 hr before challenging them with elevated (30 mM) glucose (Figure 1A). Live imaging of a fluorescent glucose sensor (Hou et al., 2011)

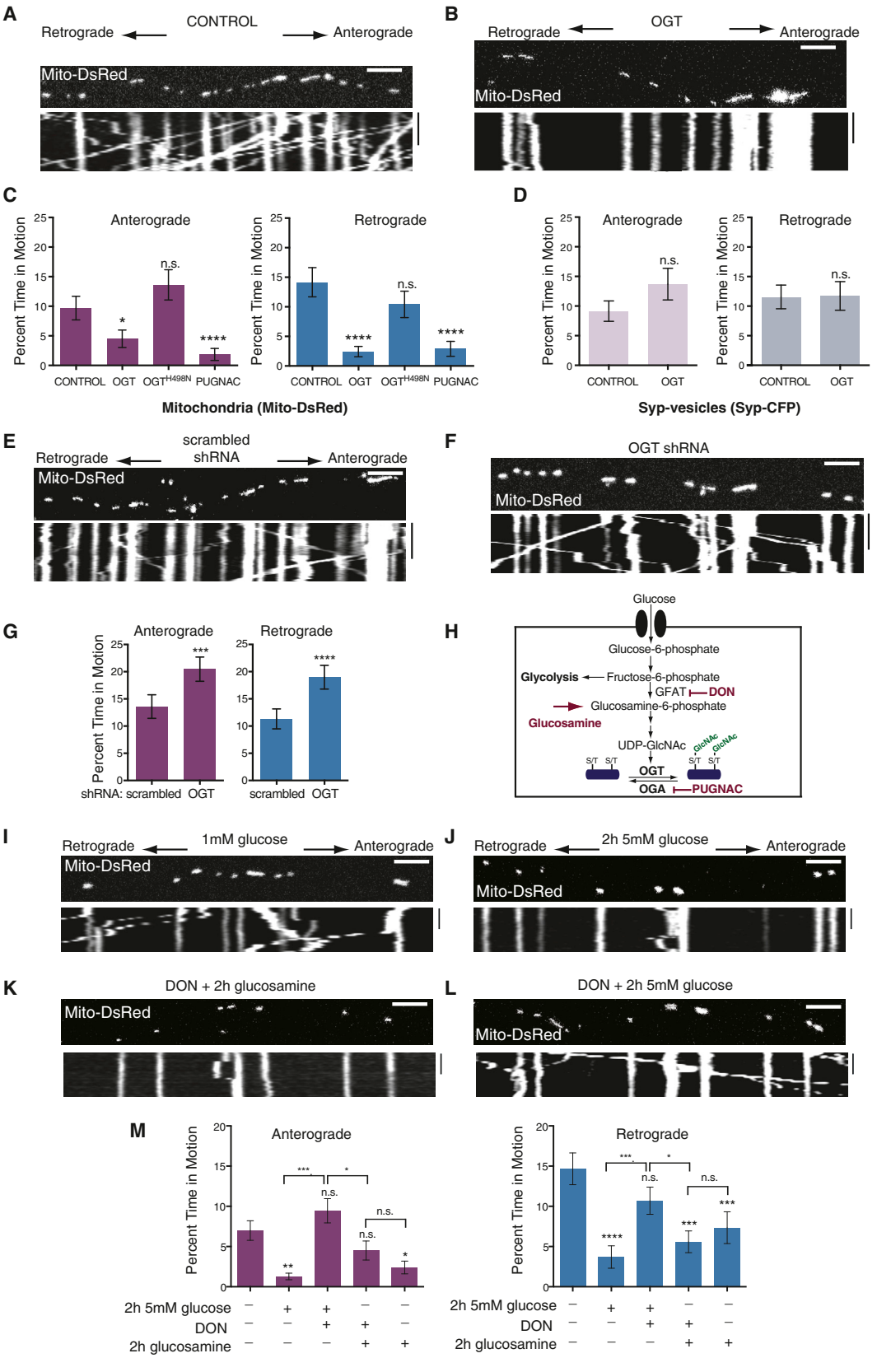

(legend on next page)

confirmed that this extracellular shift altered intracellular glucose concentration (Figures 1B and 1C). The transporter that likely mediates this increase, GLUT3, was present at neuronal cell bodies and densely spaced patches along processes (Figure S1 available online) (Choeiri et al., 2002; Ferreira et al., 2011); mitochondria throughout the cell are therefore likely to experience the shift in intracellular glucose.

To compare their dynamics in neurons maintained in 5 mM (Movies S1 and S2) or shifted to 30 mM glucose (Movies S3 and S4), we determined the percent time each mitochondrion and Syp-vesicle spent in motion, their average velocity, and total distance traveled, as well as mitochondrial length and density (Table S1). Increasing extracellular glucose reduced both anterograde and retrograde movement of mitochondria (Figures 1D–1F). Mitochondrial density also decreased in axons, potentially due to decreased movement of mitochondria into the axon from the cell body (Table S1A). The reduction was specific to mitochondria; movement of Syp-vesicles in the same axons increased significantly in both directions (Figure 1G and Table S1A) even as mitochondrial movement decreased. The enhanced movement of Syp vesicles entailed increases in velocity and total distance traveled.

Increased *O*-GlcNAc Transferase Activity Arrests Mitochondria

We hypothesized that OGT was responsible for the effect of elevated glucose on mitochondrial movement. We therefore examined the effect of OGT by transfecting neurons with the full-length nucleocytoplasmic isoform of OGT together with Mito-DsRed and Syp-CFP. OGT overexpression reduced axonal mitochondrial motility and density (Figure 2, Table S1B, and Movies S5 and S6). In contrast, OGT did not decrease the movement of Syp-vesicles. Expression of OGT^{H498N}, a mutant lacking catalytic activity (Lazarus et al., 2011) (Figure S2A), did not significantly change mitochondrial motility (Figure 2C). To increase *O*-GlcNAcylation without overexpressing OGT, we instead treated neurons with *O*-(2-acetamido-2-deoxy-D-glucopyranosylidene) amino-*N*-phenylcarbamate (PUGNAC), an inhibitor of the de-GlcNAcylating enzyme OGA. PUGNAC also reduced mitochondrial motility (Figure 2C). Thus, either the expression of catalytically active OGT or the inhibition of endogenous OGA mimicked the effect of elevated glucose on mitochondrial motility.

We also probed the influence of OGT by pharmacologically manipulating the availability of its substrate UDP-GlcNAc. UDP-GlcNAc synthesis can be blocked with 6-diazo-5-oxo-L-norleucine (DON), an inhibitor of glutamine fructose-6-phosphate amidotransferase (GFAT). We therefore cultured hippocampal neurons expressing OGT in 5 mM glucose for 72 hr either in the presence or absence of 10 μM DON. DON alone did not alter mitochondrial motility, but it prevented the inhibition of movement caused by OGT overexpression (Figures S2B–S2F). These observations were consistent with a model in which increased glucose availability stimulated OGT activity (Butkinaree et al., 2010; Love and Hanover, 2005) and thereby inhibited the movement of mitochondria.

To assess whether reducing endogenous OGT alters mitochondrial motility, we depleted OGT from neurons by coexpressing GFP with a short hairpin RNA (shRNA) against OGT (Caldwell et al., 2010). The efficacy of the shRNA was established in hippocampal neurons after 4 days of expression (Figure S2G) and in HEK293T cells (Figure S2H). OGT depletion enhanced mitochondrial motility in both directions (Figures 2E–2G and Table S1B). This enhancement was suppressed by expression of shRNA-resistant OGT (Figures S2I and S2J) and was specific to mitochondria because the retrograde trafficking of late endosomal vesicles (visualized by RFP-Rab7) was inhibited by OGT depletion (Figure S2K).

Regulation of Mitochondrial Motility in the Physiological Range of Glucose Concentrations

Although neurons are normally cultured in 25 mM glucose, extracellular glucose ranges from 2 to 6 mM in mammalian brain (Silver and Erecińska, 1994). To examine mitochondrial motility at concentrations resembling those in vivo, we cultured hippocampal neurons in 5 mM glucose containing NB medium and then lowered the glucose to 1 mM for 48 hr before challenging them with 5 mM glucose for 2 hr. 1 mM lactate and pyruvate were present throughout as alternative energy supplies that are not metabolized to UDP-GlcNAc. Shifting to higher extracellular glucose again reduced mitochondrial movement (Figures 2I, 2J, and 2M). Consistent with mediation by the HBP, the reduction was blocked by DON (Figures 2H–2M). Glucosamine, which enters the HBP downstream of GFAT, also reduced mitochondrial movement,

Figure 2. OGT and the Hexosamine Pathway Inhibit Mitochondrial Motility

(A and B) Kymographs of axons from hippocampal neurons transfected with Mito-DsRed and Syp-CFP either with (A) or without (B) OGT and imaged 3 days after the transfection.

(C and D) The percent of time mitochondria (C) and Syp vesicles (D) spent in motion was quantified from kymographs of either control cultures or neurons transfected with either OGT or the catalytically inactive OGT^{H498N} or neurons pretreated for 6 hr with 100 μM PUGNAC. n = 100–129 mitochondria from 8 axons, and n = 118–165 vesicles from 7 to 8 axons and 4 independent transfections per condition.

(E–G) Hippocampal neurons were transfected with Mito-DsRed and either a scrambled shRNA (E) or OGT shRNA (F) and imaged 4 days after the transfection, and their consequences for mitochondrial motility were quantified (G). n = 175–179 mitochondria from 9 axons and 3 independent transfections per condition.

(H) Schematic representation of glucose and glucosamine metabolism by the HBP. Rate-limiting steps and the inhibitors used in this study are also indicated.

(I–M) Hippocampal neurons, cultured in 5 mM glucose, were transfected with Mito-DsRed and transferred to media containing 1 mM glucose for 48 hr (similar to Figure 1A). Mitochondrial motility was imaged with the indicated glucose, glucosamine, and DON treatments. (I and J) Representative kymographs at 1 mM glucose and 2 hr after shift to 5 mM glucose. (K and L) Addition of the GFAT inhibitor DON (100 μM) prevented the reduction in motility caused by 5 mM glucose (L), but not by 2 hr exposure to 1 mM glucose and 4 mM glucosamine (K). (M) Mitochondrial motility was quantified from kymographs as in (I)–(L). Throughout the experiments in (I)–(M), medium was supplemented with 1 mM lactate and 1 mM pyruvate; n = 116–199 mitochondria from 8 to 13 axons and 3 to 4 independent transfections per condition.

n.s., not significant. *$p < 0.05$, **$p < 0.01$, ***$p < 0.001$, and ****$p < 0.0001$; Kruskal-Wallis test. All values are shown as mean ± SEM. Scale bars, 10 μm and 100 s. See also Figure S2, Movies S5 and S6, and Table S1B.

and, as predicted, this reduction was not blocked by DON (Figure 2M).

Milton Recruits OGT to Mitochondria and Undergoes Regulated *O*-GlcNAcylation

To determine whether the interaction with Milton caused OGT to be recruited to the mitochondrial surface, we transfected both COS7 cells and neurons with Mito-DsRed and eGFP-tagged OGT in the presence and absence of myc-hMilton1. Expression of the tagged OGT allowed us to distinguish mitochondrial binding of the nucleocytoplasmic isoform in the transgene from an intramitochondrial variant that also occurs in cells (Love and Hanover, 2005). In the absence of Milton expression, eGFP-OGT was largely diffuse in the COS7 cytosol and nucleus, although some was present on mitochondria. With Milton overexpression (Figure S3A), eGFP-OGT was highly mitochondrial. Similarly, in neuronal processes, eGFP-OGT became highly enriched on mitochondria when Milton was coexpressed (Figures 3A–3D). Miro or KHC coexpression did not enrich eGFP-OGT on mitochondria (data not shown).

To test the possibility that OGT arrests mitochondrial motility through dissociation of the Milton/KHC/Miro complex, we immunoprecipitated hMilton1 from HEK293T cells with or without overexpression of OGT. Endogenous OGT coprecipitated with hMilton1, but overexpression of OGT greatly enhanced this association (Figure 3E). However, as OGT-hMilton1 association increased, levels of coprecipitated kinesin and Miro remained constant. Moreover, immunoprecipitation of an epitope-tagged kinesin pulled down both endogenous and overexpressed OGT, together with hMilton1 (Figure S3B). Thus, association of OGT with Milton did not disrupt the mitochondrial motor/adaptor complex (Figures 3E and S3B) and OGT bound to complexes that also contain KHC.

We examined O-GlcNAcylation of myc-tagged hMilton1 to determine whether the extent of its modification was altered when OGT was overexpressed or OGA was inhibited. Anti-GlcNAc antibodies detected a band that comigrated with hMilton1 in anti-myc immunoprecipates from HEK293T cells expressing myc-tagged hMilton1 (Figure 3F). Intensity of this band was increased by inhibition of OGA by PUGNAC, overexpression of OGT, or both combined (Figures 3F and 3G), but overexpression of OGT^{H498N} did not (Figures 3H and 3I). PUGNAC also increased the GlcNAcylation state of endogenous hMilton1 (Figure S3C). Thus, GlcNAcylation sites on Milton are not saturated in control conditions, and the level of their modification is likely to be determined by the balance of OGT and OGA activity.

A Stable OGT-Milton Interaction Is Not Necessary for *O*-GlcNAcylation of Milton

Milton, unlike most other highly *O*-GlcNAcylated proteins, forms a stable immunoprecipitable complex with OGT both in vitro and in vivo (Brickley et al., 2011; Iyer et al., 2003; Iyer and Hart, 2003). To determine whether we could selectively prevent Milton *O*-GlcNAcylation by interfering with this binding, we mapped the region required for its stable association with OGT. We expressed truncated forms of both *Drosophila* MiltonA and hMilton1 in HEK293T cells and assayed their ability to coprecipitate with OGT (Figures 4A and S4A–S4C). OGT binding appeared to depend on residues between 450 and 750 of *Drosophila* MiltonA (Figure 4A) and 634–953 of hMilton1 (Figures S4A and S4B). Although these are among the less conserved regions of Milton, we identified a highly conserved 15 amino acid region (658–672 in hMilton1; Figure 4B). Deletion of these residues prevented the coprecipitation of OGT with Milton (Figure 4C). hMilton1 lacking this OGT-binding domain (hMilton1ΔOBD) retained the ability to coprecipitate with KHC and Miro and localize to mitochondria (Figures S4C–S4E). However, although hMilton1ΔOBD no longer bound OGT with sufficient affinity to coprecipitate, its *O*-GlcNAcylation by OGT was not diminished but rather increased, indicating that the high-affinity interaction interferes with its ability to modify Milton (Figures 4D and 4E). Thus, formation of a stable OGT-Milton complex is not required for Milton to serve as a substrate for OGT. The tetratricopeptide repeat (TPR) domains of OGT, however, are thought to scaffold the interactions of OGT with multiple substrates (Iyer and Hart, 2003; Lazarus et al., 2011). Deletion of the first 6 TPR domains (Δ6 TPR) decreased Milton *O*-GlcNAcylation, as anticipated (Figures 4F–4H), and this truncated OGT did not arrest neuronal mitochondria (Figures 4I–4K and Table S1C). Thus, the GlcNAcylation of Milton does not require the exceptionally stable interaction of OGT with the OBD domain on Milton but, as with other OGT substrates, requires the substrate-recognizing TPR domains of OGT.

OGT-Dependent Mitochondrial Arrest Requires Milton *O*-GlcNAcylation

We previously characterized four sites of *O*-GlcNAcylation on Milton isolated from mouse synaptosomes (Trinidad et al., 2012). To identify O-GlcNAcylation sites present in hMilton1, this protein was immunoprecipitated from HEK293T cells and resolved on an SDS-PAGE gel. Peptides isolated from a tryptic digestion were analyzed by tandem mass spectrometry (MS/MS) using electron transfer dissociation, which preserves labile glycosidic linkages. We identified eight peptides on hMilton1 that were modified with O-GlcNAc. In three of these, the modified site could be localized to a single residue (Figure S5).

To determine the potential role of these sites in mitochondrial arrest, we expressed in HEK293T cells hMilton1 constructs wherein putative *O*-GlcNAcylation sites were mutated to alanine (Figure S5 and Table S1D) and measured their relative *O*-GlcNAc levels. We focused on four *O*-GlcNAcylated serines conserved between mouse and human Milton1 (Figure 5A). Mutation of any of the four sites reduced the amount of GlcNAc immunoreactivity present on Milton (Figure 5B). The requirement for Milton *O*-GlcNAcylation in mediating the OGT-dependent mitochondrial arrest was demonstrated with a quadruple mutant that had all four of these conserved serines changed to alanine ($hMilton1^{Qmut}$). We compared the consequences of its expression to that of hMilton1 wild-type (WT) when OGT was coexpressed. Therefore, we used hMilton1 DNA at a low concentration (0.2 μg/well of a 24-well plate) to minimize the increase in motility caused by high levels of Milton (Glater et al., 2006). By immunostaining, 96% ± 2.27% of neurons that were Mito-DsRed positive were also myc-hMilton1 and OGT positive (Figure S5I). The quadruple mutation, expressed on its own, increased mitochondrial length by 20% but had little effect on the parameters

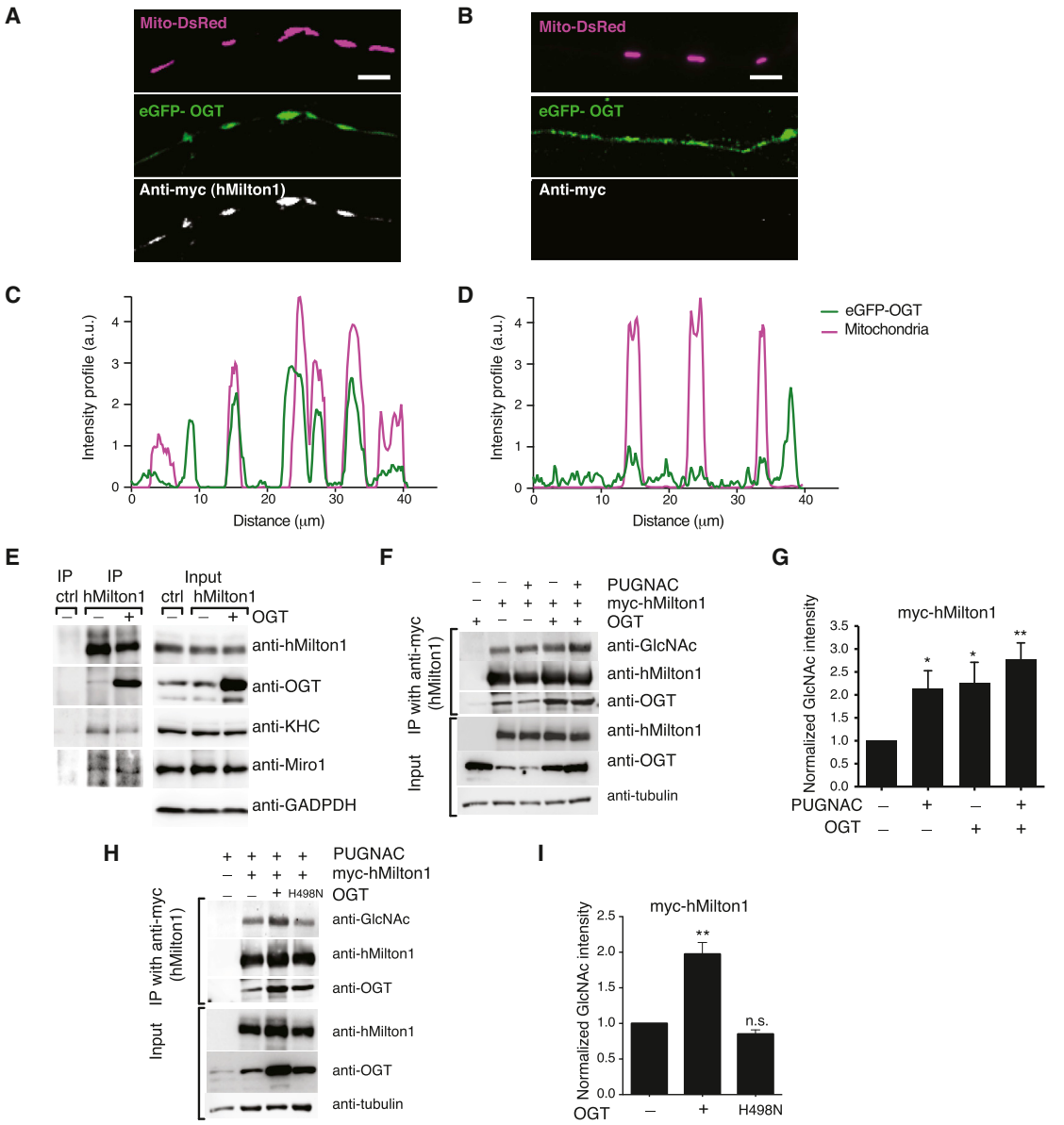

Figure 3. OGT and OGA Regulate hMilton1 *O*-GlcNAcylation

(A–D) Milton expression recruits OGT to axonal mitochondria. Hippocampal axons were cotransfected with eGFP-OGT, Mito-DsRed, and either an empty vector (A and C) or myc-hMilton1 (B and D), and immunofluorescent intensity for eGFP-OGT and Mito-DsRed was measured along the length of the axons shown.

(E) Immunoprecipitation (IP) of endogenous hMilton1 from HEK293T cells to analyze the consequences of OGT overexpression. Precipitation with rabbit IgG was used as a control. Input lanes were loaded with 3% of the cell lysates used for the IP and also probed with anti-GAPDH antibody as a loading control. OGT overexpression increased its coprecipitation with Milton without decreasing the presence of Miro or KHC in the complex. A lower OGT-immunoreactive band in the input lanes arises from the intramitochondrial isoform of OGT, which is not coprecipitated with hMilton1.

(F–I) Regulation of hMilton1 *O*-GlcNAcylation in HEK293T cells. Cells were transfected and treated as indicated. (F) myc-hMilton1 was immunoprecipitated with anti-myc from cells treated overnight with 100 μM PUGNAC and/or overexpressing OGT. With fluorescently tagged secondary antibodies, band intensities were quantified (G) in the linear range, and the intensity of each GlcNAc band was normalized to the intensity of myc bands. GlcNAc levels on myc-hMilton1 in untreated cells were set as 1, and fold changes in response to PUGNAC treatment and OGT overexpression were calculated. n = 4 independent transfections per condition. (H and I) myc-hMilton1 was immunoprecipitated from HEK293T cells with or without overexpression of OGT or catalytically dead OGT^{H498N} and its GlcNAcylation quantified as in (G). n = 3 independent transfections per condition.

n.s., not significant. *p < 0.05 and **p < 0.01; one-way ANOVA. All values are shown as mean ± SEM. Scale bar, 10 μm. See also Figure S3.

of mitochondrial movement when compared to WT Milton expression (Table S1E) and therefore allowed a straightforward comparison of the effect of OGT expression on mitochondria bearing either form of Milton. Three concentrations of OGT DNA were used for transfections so as to construct a dose/response relationship. As expected, mitochondrial motility

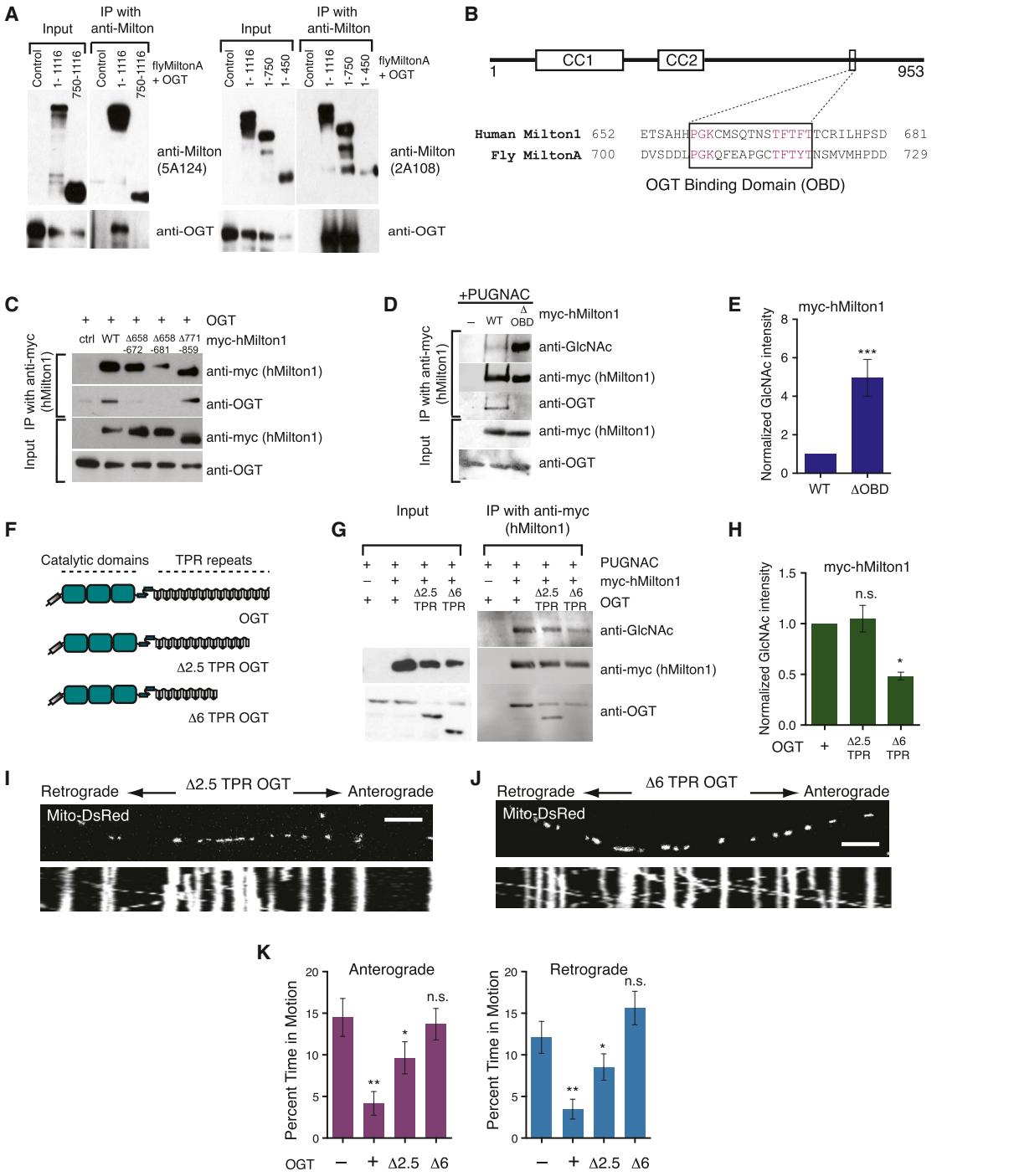

Figure 4. An OGT/Milton Complex Is Not Required for hMilton1 *O*-GlcNAcylation

(A) Coimmunoprecipitation of full-length or truncated fly MiltonA and OGT proteins from HEK293T cells. Anti-*Drosophila* Milton antibodies 5A124 (raised against amino acids 908–1055) or 2A108 (raised against amino acids 273–450) were used to immunoprecipitate full-length (1–1,116) or truncated (750–1,116, 1–750, and 1–450) *Drosophila* MiltonA. Immunoblots were probed with anti-OGT and the appropriate anti-Milton antibodies to identify Milton fragments that could associate with OGT.

(B) Schematic representation of hMilton1 protein and sequence alignment of fly MiltonA (450–750) and hMilton1 (634–953) (see also Figure S4), which were determined to be important for OGT/Milton complex formation. The conserved OBD is boxed; conserved amino acids are magenta. Predicted coiled-coil domains of hMilton1 (CC1,2) are also illustrated.

(C) Myc-hMilton1 constructs lacking the indicated amino acids were tested for their ability to precipitate coexpressed OGT from HEK293T cells.

(legend continued on next page)

decreased in both control and hMilton1 WT-expressing neurons as we increased the amount of transfected OGT DNA (Figures 5D, 5E, and 5H and Table S1E). However, when hMilton1^{Qmut} was expressed, OGT expression had no effect on their motility, even when the highest concentration of OGT DNA was transfected (Figures 5F–5H, Table S1E, and Movie S7). hMilton1^{Qmut} prevented the arrest whether or not the endogenous murine Milton was knocked down by shRNA (Figures S5J and S5K). We also analyzed mitochondrial motility in neurons expressing hMilton1 S447A, S829/30A, or S938A together with OGT overexpression or PUGNAC treatment (Figure S5L). The individual mutations were also effective in rendering motility resistant to OGT. Understanding the significance of individual sites will require further elucidation of this mechanism.

Glucose-Dependent Changes in Mitochondrial Motility Require Milton *O*-GlcNAcylation

Identification of the required *O*-GlcNAcylation sites on hMilton1 allowed us to use the protocol in Figure 1A to determine whether this modification mediated the effect of increased extracellular glucose. High glucose decreased movement in hippocampal neurons expressing WT hMilton1 (Figures 6A, 6B, and 6E and Table S1F). In contrast, motility increased in neurons expressing hMilton1^{Qmut} (Figures 6C–6E and Table S1F), particularly in the anterograde direction. Thus, the suppression of mitochondrial movement is mediated by the GlcNAcylation of Milton. In its absence, mitochondria behave akin to the Syp vesicles of Figure 1, whose motility was enhanced when more glucose was available. To determine the *O*-GlcNAcylation state of Milton under different extracellular glucose conditions, we expressed myc-tagged WT or Qmut hMilton1 constructs in HEK293T cells. High glucose only increased the *O*-GlcNAcylation level of WT hMilton1 (Figures 6F and 6G).

Loss of OGT Decreases the Stationary Mitochondrial Pool In Vivo

Because the interaction of OGT with Milton is conserved (Figure 4A) (Glater et al., 2006), we took advantage of available *Drosophila* lines to ask whether OGT was regulating mitochondrial movement in vivo. A *piggy*Bac insertion into the *ogt* coding sequence (*ogt*$^{-/-}$) (Schuldiner et al., 2008; ID:LL01151) abolished detectable OGT protein (Figure S6A). Individual axons in segmental nerves (Schuldiner et al., 2008; Wang and Schwarz, 2009a) of *ogt*$^{-/-}$ larvae had fewer stationary mitochondria (Figures 7A–7C) and fewer mitochondria per micron of axon than control larvae (Figure S6B). These results in vivo in *Drosophila* parallel the effects of OGT knockdown in cultured hippocampal neurons and indicate a conserved role of O-GlcNAc cycling in regulating mitochondrial motility.

Milton *O*-GlcNAcylation Levels in Mouse Brain Are Altered by Feeding

In tissue culture, changes in extracellular glucose altered the extent of Milton GlcNAcylation (Figures 6F and 6G). To determine whether it also varied in vivo, we took advantage of the fact that the concentration of extracellular glucose in the brain changes in parallel with blood glucose during fasting and feeding cycles (Silver and Erecińska, 1994). Mice were either (1) fed ad libitum, (2) fasted for 24 hr, or (3) fasted for 24 hr and then returned to food for 24 hr (Figure 7D), after which their blood glucose was monitored and cerebral cortices were removed to measure Milton *O*-GlcNAcylation (Figures 7E and 7F). Although the drop in blood glucose that accompanied fasting did not produce a parallel decrease in Milton GlcNAcylation, refeeding following the fasting significantly increased it.

Axonal Mitochondria Accumulate in Areas of Higher Glucose

One possible consequence of the OGT pathway is that moving mitochondria would tend to stop where cytosolic glucose is elevated. To determine whether spatial inhomogeneities of glucose could alter mitochondrial distribution in an axon, we used microfluidic chambers to create a boundary between a zone with 5 mM glucose and one with glucose-free medium (Figures 7G and S6C). Because the glucose transporter will effectively clamp the local cytoplasmic concentration at equilibrium with the external glucose, a local difference in cytoplasmic glucose should also arise. Hippocampal neurons were cultured in chambers in 5 mM glucose and were allowed to grow their axons through 0.45 mm grooves into an axonal chamber (Figure 7G). Trypan blue was used to confirm that fluidic isolation of the axonal compartment was preserved during medium exchanges (Figure S6C). To create the glucose differential, the somal compartment was switched to glucose-free medium, whereas the axonal compartment remained in 5 mM glucose. A stretch of axon on the 5 mM glucose side of the glucose discontinuity was imaged before and after the solution change (Figure 7G). Lowering glucose in the somal compartment caused an accumulation of mitochondria in this adjacent area of higher glucose (Figures 7I and 7J). This accumulation is consistent with a model in which the mobile mitochondria from the glucose-free compartment arrest when they encounter the region with higher glucose.

(D and E) Full-length and Δ658-672 (ΔOBD) hMilton1 were immunoprecipitated from 100 μM PUGNAC-treated HEK293T cells, and *O*-GlcNAcylation was quantified as in Figure 3. Loss of the high-affinity interaction increased Milton *O*-GlcNAcylation. n ≥ 3 independent transfections per condition.
(F–H) Full-length and truncated OGT constructs lacking either the first 2.5 or 6 TRP motifs (Δ2.5, Δ6 as shown in F) were coexpressed in HEK293T cells with full-length hMilton1 (WT) to evaluate the significance of the TPR motifs on OGT/Milton complex formation and the level of hMilton1 *O*-GlcNAcylation. myc-hMilton1 was immunoprecipitated, and immunoblots were analyzed with anti-GlcNAc, anti-myc, and anti-OGT. n = 3 independent transfections per condition.
(I–K) Hippocampal neurons were transfected with Mito-DsRed and either full-length or Δ2.5 or Δ6 truncated OGT and imaged 3 days after transfection. From kymographs as in (I and J), mitochondrial motility was quantified (K) and compared with control. n = 111–209 mitochondria from 10 to 12 axons and 3 independent transfections per condition. n.s., not significant. *$p < 0.05$ and **$p < 0.01$; one-way ANOVA, Kruskal-Wallis test. All values are shown as mean ± SEM. Scale bar, 10 μm and 100 s.
See also Figure S3 and Table S1C.

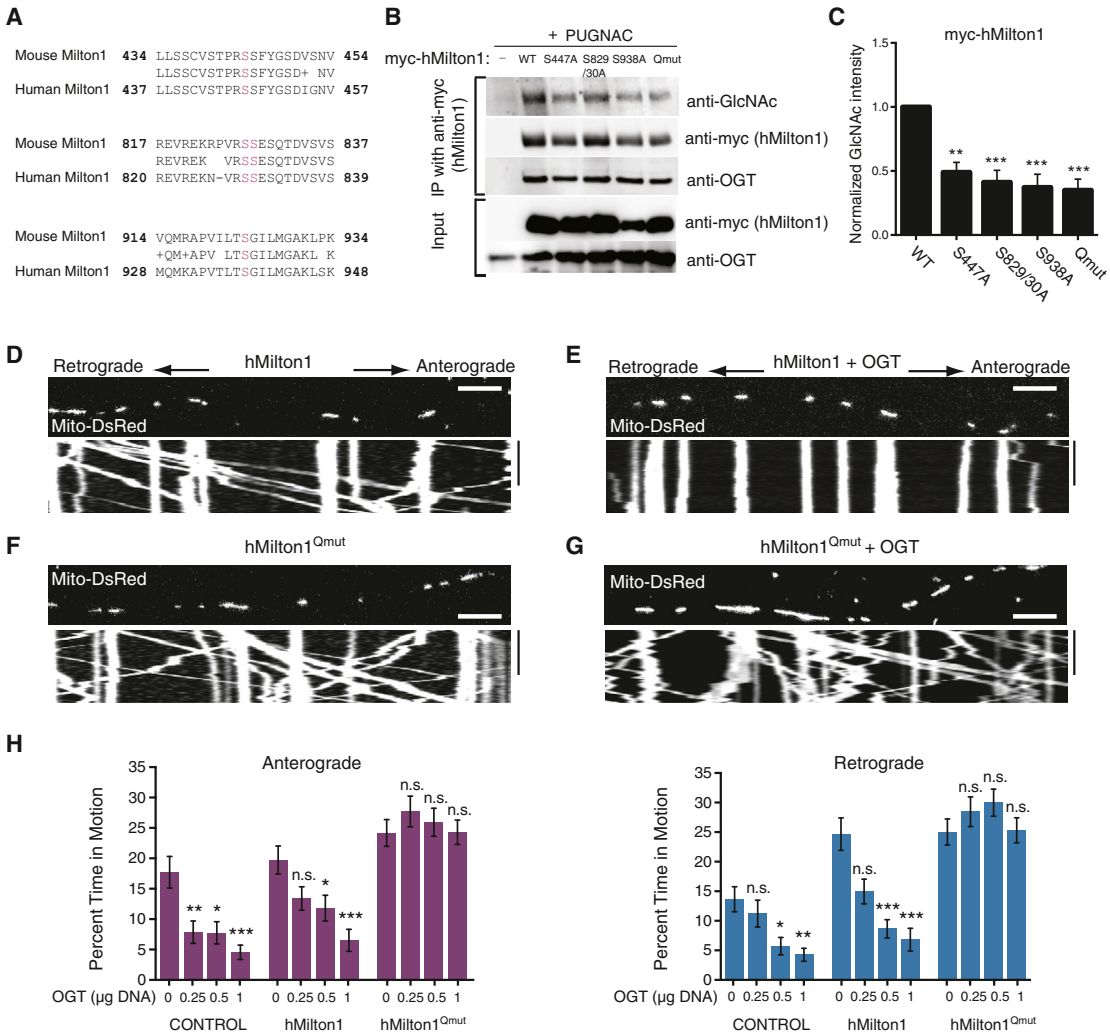

Figure 5. OGT-Dependent Mitochondrial Motility Arrest Requires Milton *O*-GlcNAcylation

(A) Sequence alignment of *O*-GlcNAcylation sites (magenta) in mouse Milton1 with homologous regions in hMilton1 (see also Figure S5 and Table S1D).

(B and C) Myc-hMilton1 with either individual putative GlcNAc sites mutated or the quadruple mutant lacking all four sites (Qmut) or WT were expressed in HEK293T cells and cultured overnight with 100 μM PUGNAC. Milton immunoprecipitates were probed with anti-GlcNAc, anti-myc, and anti-OGT antibodies, and GlcNAcylation levels on Milton were quantified with fluorescently tagged secondary antibodies. The intensity of each GlcNAc band was normalized to the intensity of the myc band, with the baseline hMilton1 GlcNAc level set as 1 to reveal relative changes. n ≥ 3 independent transfections per condition.

(D–G) Hippocampal neurons were transfected with Mito-DsRed and the indicated forms of hMilton1 with (E and G) or without (D and F) OGT (0.5 μg OGT DNA/well). Mitochondrial motility was imaged 3 days after transfection. (H) To assess the effect of the mutated GlcNAcylation sites, a dose/response relationship was established with different levels of DNA for OGT transfection and its effect on mitochondrial motility quantified from kymographs as in (D)–(G). The amount of OGT DNA transfected per well of a 24-well plate is indicated. n = 75–174 mitochondria from 8 to 9 axons and 3 independent transfections per condition. All values are shown as mean ± SEM. The significance of changes in motility was determined relative to the motility in neurons expressing the same Milton construct without OGT transfection. n.s., not significant. *$p < 0.05$, **$p < 0.01$, and ***$p < 0.001$; one-way ANOVA, Kruskal-Wallis test. Scale bar, 10 μm and 100 s. See also Figure S5, Movie S7, and Table S1E.

DISCUSSION

Mitochondrial movement controls their distribution in cells, their likelihood of fusing, and their rate of turnover in the cell periphery. The control of mitochondrial movement can therefore influence energy, signaling, metabolism, and Ca^{2+} buffering in different regions of a cell (Saxton and Hollenbeck, 2012). We have now established (1) that extracellular glucose regulates mitochondrial dynamics; (2) that the enzyme OGT, a putative metabolic sensor, mediates this effect; (3) that a posttranslational modification of Milton is an absolutely required target of this enzyme, and (4) that the pathway is likely to be physiologically relevant in vivo for regulating mitochondrial dynamics and distribution.

The GlcNAcylation level of Milton correlated well with mitochondrial motility, whether the level was manipulated by overexpression or knockdown of OGT, or by pharmacological inhibition

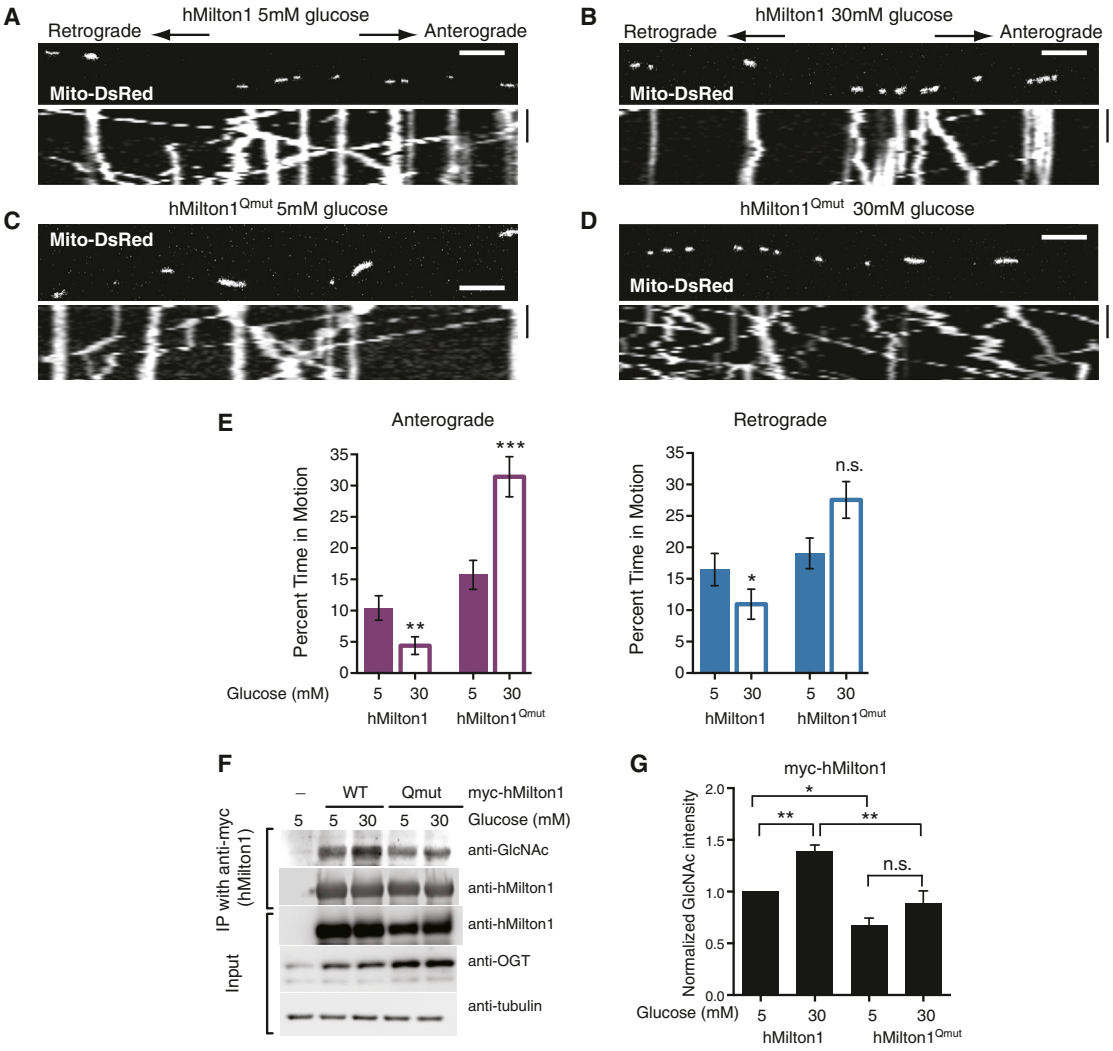

Figure 6. Milton *O*-GlcNAcylation Is Necessary for Glucose to Decrease Mitochondrial Movement

(A–D) Hippocampal neurons were transfected with Mito-DsRed and either WT or Qmut hMilton1 constructs as indicated and cultured as per the protocol described in Figure 1A.

(E) Percent time each mitochondrion spent in anterograde and retrograde motion was calculated from kymographs as in (A)–(D). n = 105–135 mitochondria from 9 axons and 3 independent transfections per condition. Scale bar, 10 μm and 100 s. See also Table S1F.

(F and G) WT or Qmut myc-hMilton1 were expressed in HEK293T cells cultured in 25 mM glucose containing DMEM. Glucose levels were then lowered to 5 mM for 24 hr before challenging them with 30 mM or 5 mM glucose for 2 hr as in the motility experiments. Milton immunoprecipitates were probed with anti-GlcNAc, anti-myc, and anti-OGT antibodies (F), and GlcNAcylation levels on Milton were quantified (G). n = 4 independent transfections per condition.

All values are shown as mean ± SEM; n.s., not significant. *p < 0.05, **p < 0.01, and ***p < 0.001; Mann-Whitney *U* test, one-way ANOVA.

of OGA or UDP-GlcNAc synthesis (Figure 2). OGT has many substrates, including several such as tubulin, kinesin, and dynein with potential impact on mitochondrial dynamics (Ji et al., 2011; Ruan et al., 2012; Trinidad et al., 2012). However, by mapping and mutating four key sites of GlcNAc addition in hMilton1 (hMilton1^{Qmut}), we demonstrated that Milton is the key and essential substrate through which OGT inhibits mitochondrial motility. These mutations had little effect on the baseline properties of mitochondrial movement but selectively prevented the arrest by OGT (Figure 5). With hMilton1^{Qmut} expression, we also found that GlcNAcylation of Milton mediated the decrease in mitochondrial movement caused by elevated extracellular glucose (Figure 6). Moreover, although, in this study, we took advantage of the polarized arrays of microtubules in axons, the components of this pathway are present in all metazoan cells and glucose, via OGT, may therefore be a widespread regulator of mitochondrial movement.

Protein GlcNAcylation is a posttranslational modification that occurs on more than 1,000 proteins and has received much recent attention (Ruan et al., 2013). OGT has low-affinity interactions with many of its substrates but forms a stable complex with few. Milton was one of the first identified high-affinity OGT partners (Iyer et al., 2003; Iyer and Hart, 2003), and we have identified a 15 amino acid region in hMilton1 (aa 658–672) that is required

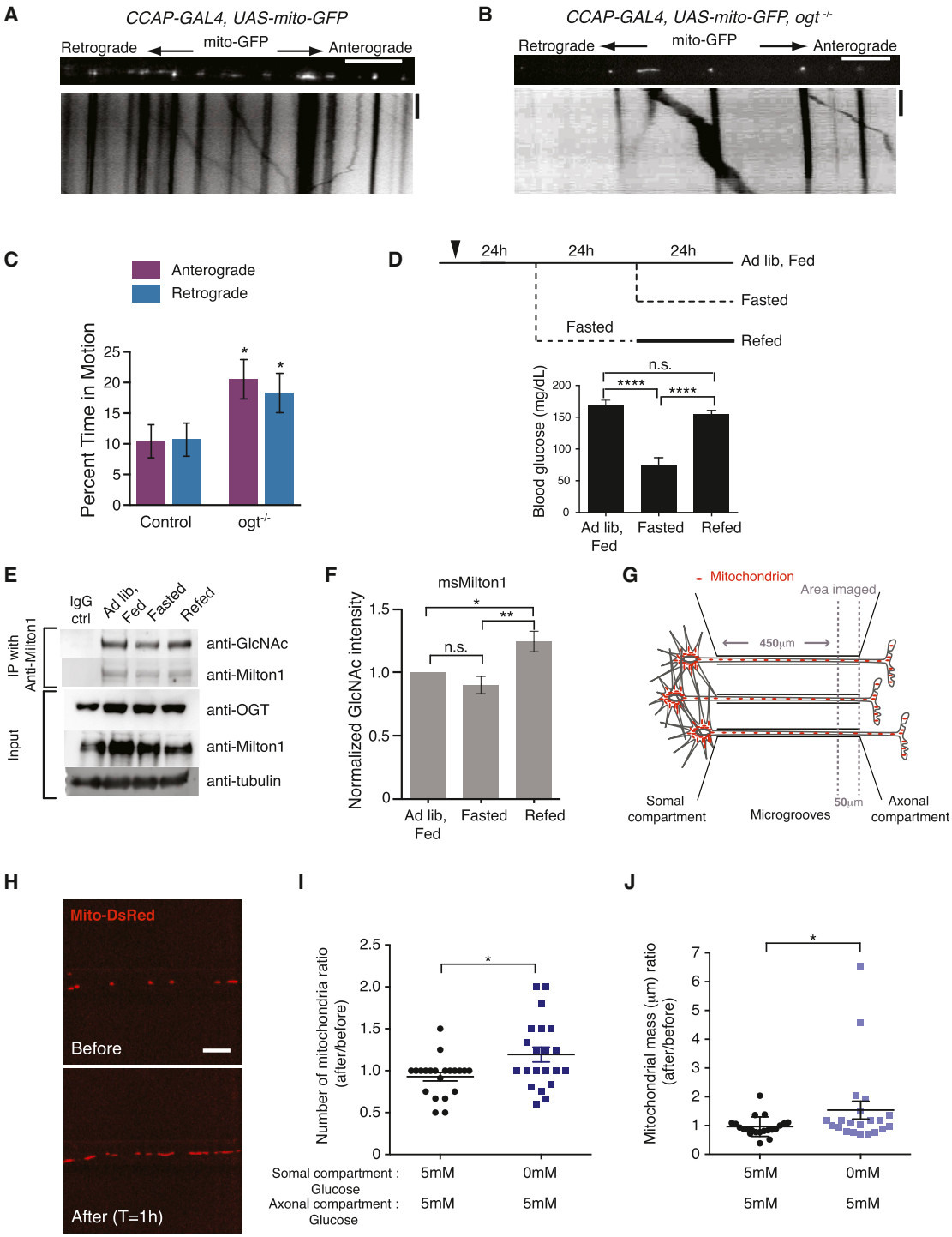

Figure 7. Evidence of OGT-Dependent Regulation of Milton *O*-GlcNAcylation In Vivo

(A and B) In control and *ogt*$^{-/-}$ larvae, UAS-mito-GFP was expressed in an identified peptidergic axon within the segmental nerve by CCAP-GAL4.

(C) The percent time each mitochondrion spent in anterograde and retrograde motion was calculated from kymographs as in (A) and (B). n = 91–100 mitochondria from 9 axons from 9 animals. Scale bar, 10 μm and 100 s.

(D) Schematic of the experimental regimen for changing blood glucose levels by fasting and refeeding and measured blood glucose levels from the mice that were used to compare Milton *O*-GlcNAcylation levels in the brain.

(E and F) Immediately after blood glucose measurements, two cortical hemispheres were removed and homogenized. Milton1 was immunoprecipitated (E), and GlcNAcylation levels on Milton were quantified (F). n = 6 pairs of animals.

(legend continued on next page)

for stable OGT-Milton complexes (Figures 5 and S4). However, deletion of this region does not reduce hMilton1 O-GlcNAcylation (Figure 5D) on the critical sites. A similar dissociation of OGT binding and *O*-GlcNAcylation has been described for HCF-1 (Capotosti et al., 2011). OGT-Milton complexes may facilitate OGT transport throughout cells or target OGT to the mitochondrial surface (Figure S3) for additional metabolic regulation.

O-GlcNAcylation, like phosphorylation, modifies serine and threonine side chains; crosstalk and competition between phosphorylation and *O*-GlcNAcylation may be important for some substrates (Hart et al., 2011). Twenty-eight hMilton1 phosphorylation sites have been previously identified (Hornbeck et al., 2012), and we have mapped additional sites; however, no phosphorylation has been found at the critical *O*-GlcNacylation sites that regulate mitochondrial motility.

Some GlcNAcylation sites turn over very slowly and may serve a primarily structural role, whereas others are actively cycled and likely regulate protein function (Khidekel et al., 2007). Only for the latter class will PUGNAC inhibition of OGA cause the level of *O*-GlcNAcylation to rise (Khidekel et al., 2007; Matthews et al., 2007; Yi et al., 2012). Milton modification meets this criterion (Figures 3F and 3G), and OGA inhibition decreased mitochondrial motility (Figure 2C). Thus, the GlcNAc sites on Milton are undergoing dynamic regulation and normally exist in a substoichiometric level of modification that allows the motor/adaptor complex to respond to changes in glucose availability.

The inhibitory effect of increased extracellular glucose on mitochondrial movement was not shared by Syp-vesicles in the same axons, although both organelles use dynein for retrograde movement. Indeed, the movement of Syp vesicles was increased when glucose was raised (Figure 1). Mechanistically, this distinction is explained by two factors. (1) The locus of the inhibitory regulation is not in the motors themselves but in Milton, which is specific to mitochondria. (2) Changing extracellular glucose from 5.5 to 30 mM has been calculated to increase ATP 3-fold in hippocampal neurons (Huang et al., 2007), and raising ATP levels enhances the activity of kinesin and dynein, which require ATP hydrolysis for force generation (Fort et al., 2011; Visscher et al., 1999). Therefore, in the absence of the overriding influence of Milton GlcNAcylation, cargo transport will increase with increased glucose availability, a phenomenon we also observed for mitochondria when the action of OGT was prevented by expression of hMilton1^{Qmut} (Figure 6). Local microdomains of ATP can affect the velocity and extent of vesicle motility. Organelles can increase the efficiency of their transport by carrying their own ATP-generating machinery and mitochondrial motors require ATP produced by mitochondria (Zala et al., 2013).

The OGT pathway can now be added to a growing list of signaling cascades that regulate the motile pool of mitochondria, including changes in cytosolic Ca^{2+} (Macaskill et al., 2009; Wang and Schwarz, 2009b), growth factors and their downstream kinases (Chada and Hollenbeck, 2003), hypoxia (Li et al., 2009), Armcx (López-Doménech et al., 2012), and the PINK1/Parkin pathway (Wang et al., 2011). It is noteworthy, however, that although each of these pathways can increase the number of stationary mitochondria, they do not account for the majority of stationary mitochondria in an axon. In *Drosophila* lacking OGT, 60% of the mitochondria remained stationary (Figures 7A–7C). Similarly, ~60% of axonal mitochondria remained stationary upon knockdown of OGT or block of UDP-GlcNAc synthesis (Figure 2), and a similar fraction is stationary upon expression of Ca^{2+}-resistant Miro or mutation of PINK1 or Parkin (Wang and Schwarz, 2009b; Wang et al., 2011). This persistently stationary mitochondrial pool is dependent on anchoring proteins, including Syntaphilin (Kang et al., 2008) and Myosin VI (Pathak et al., 2010). This distinction between anchored mitochondria unchanged by short-term signals and a mobile pool that can be arrested when necessary may help the cell balance an adequate baseline of mitochondria throughout the cell while fine-tuning their distribution via the mobile pool as nutrient supply and energetic demand fluctuate.

In this study, we determined that the OGT/*O*-GlcNAcylation pathway enables neuronal mitochondrial motility to respond to changes in glucose availability. Although most measurements were conducted in cultured cells where glucose availability can readily be altered, our data indicate that the pathway also functions in vivo. In *Drosophila*, removal of OGT increased the fraction of mobile mitochondria, demonstrating that there is a tonic inhibition by the OGT pathway (Figures 7A–7C). In addition, we demonstrated that the extent of GlcNAcylation of Milton in mouse brain in vivo could vary—the increase in glucose availability upon feeding previously fasted mice increased the level of Milton *O*-GlcNAcylation (Figures 7D–7F). In principle, the pathway in vivo could respond to either spatial differences or temporal changes in glucose concentration and has the potential to enrich mitochondria in subcellular locations of high glucose for efficient ATP production. Indeed, when we created a differential in glucose concentration in microfluidic chambers, mitochondrial density increased where glucose was high. Little is known about cytoplasmic glucose concentrations in neurons, but the inhomogeneous distribution of glucose transporters (Gerhart et al., 1992) and OGT and OGA (Akimoto et al., 2003; Cole and Hart, 2001; Tallent et al., 2009) in vivo suggests that both the glucose supply and key enzymes may be heterogeneously distributed. In addition, some parts of neurons likely have better

(G) Schematic of the microfluidic-based culture platform. The culture chamber consists of fluidically isolated somal and axonal compartments connected by microgrooves. Glucose levels in the axonal and somal compartments were independently manipulated, and mitochondria were imaged in a 50 μm length of axon at the proximal end of the axonal compartment.

(H–J) Hippocampal neurons, cultured in microfludic devices in 5 mM glucose (with 1 mM lactate and pyruvate), were transfected with Mito-DsRed. The medium in the somal compartment was replaced with either the same solution or with a glucose-free medium (with 1 mM lactate and pyruvate). The same axons were imaged both before and 1 hr after this solution change (H) so that its effect on mitochondrial density and mass could be quantified (I and J). n = 21 axons, 4 microfluidic devices per condition, 3 independent experiments.

All values are shown as mean ± SEM; n.s., not significant. *p < 0.05 and ****p < 0.0001; Mann-Whitney *U* test, one-way ANOVA, Kruskal-Wallis test. See also Figure S6.

access to extracellular glucose, such as nodes of Ranvier or areas close to blood vessels. Altered distribution of mitochondria is only one likely consequence; because mitochondrial fusion is highly dependent on their motility, increased Milton GlcNAcylation is likely to decrease fusion and the exchange of components and have consequences for metabolism (Liesa and Shirihai, 2013; Liu and Hajnóczky, 2011). Temporal changes in glucose availability are also relevant to neuronal metabolism. In both the central and peripheral nervous system, fasting and feeding alters levels of extracellular glucose (Choeiri et al., 2002; Dash et al., 2013; Silver and Erecińska, 1994). Furthermore, during synaptic activity and action potential firing, surface glucose transporter levels and hence glucose uptake is increased, as is ATP consumption (Ferreira et al., 2011; Weisová et al., 2009). Thus, during intense synaptic activity, the local activation of OGT and *O*-GlcNAcylation of Milton would cause existing mitochondria to be retained at pre- and postsynaptic sites and would capture any nearby transiting mitochondria. The resulting enrichment for mitochondria would enhance ATP production and Ca^{2+} buffering to preserve synaptic efficacy. On the other hand, poorly regulated blood glucose gives rise to diabetic neuropathy, and it is tempting to speculate that misregulation of mitochondrial motility in peripheral axons, via the pathway described here, could cause insufficient turnover of peripheral mitochondria and thereby contribute to axonal degeneration.

EXPERIMENTAL PROCEDURES

Plasmid Constructs

Standard PCR-based cloning strategies were used (see the Extended Experimental Procedures).

Cell Culture and Transfection

HEK293T and COS7 cells were cultured in DMEM supplemented with L-glutamine, penicillin/streptomycin (Life Technologies), and 10% FBS (Atlanta Premium). Plasmid DNA transfections were performed with the calcium phosphate method. When used, PUGNAC (Tocris Bioscience) was applied at 100 μM for 12–20 hr before cell lysis.

Hippocampal neurons were isolated from E18 rat (Charles River) embryos as previously described (Nie and Sahin, 2012) and plated at 5–7 × 10^4/cm^2 density on coverslips (Bellco Glass) coated with 20 μg/ml poly-L-ornithine (Sigma) and 3.5 μg/ml laminin (Life Technologies) and maintained in NB medium supplemented with B27 (Life Technologies), L-glutamine, and penicillin/streptomycin, unless modified as specified. Seven to ten DIV hippocampal neurons were transfected using Lipofectamine2000 (Life Technologies) and imaged 2–3 days later. The coexpression of multiple constructs transfected into neurons was validated by retrospective immunostaining following live-cell imaging. For particular treatments of neuronal cultures, see the Extended Experimental Procedures.

Live-Cell Imaging and Motility Analysis

For live-cell imaging of axonal mitochondria and Syp-vesicles, coverslips were transferred to HibernateE (BrainBits) medium to maintain cell viability in CO_2-free conditions. Kymographs were generated from 3- to 5-min-long time-lapse movies and analyzed with Kymolyzer, a custom-written ImageJ macro (see the Extended Experimental Procedures for details) for percent time in motion, velocity, total distance traveled, mitochondrial density, and length.

Immunocytochemistry and Protein Analyses

Hippocampal neurons and COS7 cells were fixed and immunostained as previously (Glater et al., 2006; Stowers et al., 2002) with the indicated antibodies (see the Extended Experimental Procedures). Images were processed with ImageJ (Schneider et al., 2012) using only linear adjustments of contrast and color. HEK293T cells lysis and immunoprecipitations were performed as previously with minor modifications (Glater et al., 2006). For immunodetection and hMilton1 GlcNAcylation measurements from immunoprecipitates, see the Extended Experimental Procedures.

Drosophila Stocks and Mitochondrial Motility Analysis

The following *Drosophila* stocks were used: *CCAP-GAL4* (Park et al., 2003), *UAS-mito-GFP* (Pilling et al., 2006), and $ogt^{-/-}$ (Schuldiner et al., 2008). Dissected third-instar larvae were imaged in a chamber on a glass slide. Kymographs were generated and analyzed as described previously (Wang and Schwarz, 2009a).

Statistical Analysis

Throughout the paper, data are expressed as mean ± SEM. Statistical analysis was performed with GraphPad Prism v6.0 for MacOSX. The Mann-Whitney *U* test was used to determine the significance of differences between two conditions. Multiple conditions were compared by Kruskal-Wallis nonparametric ANOVA test, which was followed by Dunn's multiple comparisons test or by one-way ANOVA with post hoc Tukey's test as appropriate to determine significance of differences across every condition to control condition. $p < 0.05$ was considered significant.

SUPPLEMENTAL INFORMATION

Supplemental Information includes Extended Experimental Procedures, six figures, one table, and seven movies and can be found with this article online at http://dx.doi.org/10.1016/j.cell.2014.06.007.

ACKNOWLEDGMENTS

We gratefully acknowledge the gift of plasmid constructs from Drs. P. Aspenström for myc-hMiro1/2; G. Hajnóczky for Mito-DsRed; G.W. Hart for OGT and Xpress-hMilton1; X. Yang for eGFP-OGT; H.T. Cline for Syp-CFP; M. Sahin for scrambled shRNA; M.J. Reginato for OGT shRNA; K.J. Verhey for KHC-mCit; and M. Greenberg for pEGFP-N1. We thank S. Vasquez, K. Pereira, K. Apaydin, and Dr. M. Sahin's laboratory for assistance with primary hippocampal neuron cultures; X. Ho, E. Ling, and Y. Guo for technical assistance; L. Ding from Harvard NeuroDiscovery Center, Enhanced Neuroimaging Core for assistance with development of Kymolyzer; the IDDRC Molecular Genetics and Imaging Cores (grant number P30HD18655). We also thank Drs. M. Banghart, R. Cartoni, M.A. Cronin, B. Lowell, G. Yellen, and M. Tantama and A. Nasser and M. Hamilton for support and valuable input. D.K. was supported by K01DK094943 and P30DK46200. This work was supported by 5R01GM069808-08 and the Ellison Medical Foundation.

Received: May 13, 2013
Revised: February 20, 2014
Accepted: April 28, 2014
Published: July 3, 2014

REFERENCES

Akimoto, Y., Comer, F.I., Cole, R.N., Kudo, A., Kawakami, H., Hirano, H., and Hart, G.W. (2003). Localization of the O-GlcNAc transferase and O-GlcNAc-modified proteins in rat cerebellar cortex. Brain Res. *966*, 194–205.

Brickley, K., Pozo, K., and Stephenson, F.A. (2011). N-acetylglucosamine transferase is an integral component of a kinesin-directed mitochondrial trafficking complex. Biochim. Biophys. Acta *1813*, 269–281.

Butkinaree, C., Park, K., and Hart, G.W. (2010). O-linked beta-N-acetylglucosamine (O-GlcNAc): Extensive crosstalk with phosphorylation to regulate signaling and transcription in response to nutrients and stress. Biochim. Biophys. Acta *1800*, 96–106.

Caldwell, S.A., Jackson, S.R., Shahriari, K.S., Lynch, T.P., Sethi, G., Walker, S., Vosseller, K., and Reginato, M.J. (2010). Nutrient sensor O-GlcNAc transferase regulates breast cancer tumorigenesis through targeting of the oncogenic transcription factor FoxM1. Oncogene *29*, 2831–2842.

Capotosti, F., Guernier, S., Lammers, F., Waridel, P., Cai, Y., Jin, J., Conaway, J.W., Conaway, R.C., and Herr, W. (2011). O-GlcNAc transferase catalyzes site-specific proteolysis of HCF-1. Cell *144*, 376–388.

Chada, S.R., and Hollenbeck, P.J. (2003). Mitochondrial movement and positioning in axons: the role of growth factor signaling. J. Exp. Biol. *206*, 1985–1992.

Chang, D.T., Honick, A.S., and Reynolds, I.J. (2006). Mitochondrial trafficking to synapses in cultured primary cortical neurons. J. Neurosci. *26*, 7035–7045.

Choeiri, C., Staines, W., and Messier, C. (2002). Immunohistochemical localization and quantification of glucose transporters in the mouse brain. Neuroscience *111*, 19–34.

Cole, R.N., and Hart, G.W. (2001). Cytosolic O-glycosylation is abundant in nerve terminals. J. Neurochem. *79*, 1080–1089.

Dash, M.B., Bellesi, M., Tononi, G., and Cirelli, C. (2013). Sleep/wake dependent changes in cortical glucose concentrations. J. Neurochem. *124*, 79–89.

Ferreira, J.M., Burnett, A.L., and Rameau, G.A. (2011). Activity-dependent regulation of surface glucose transporter-3. J. Neurosci. *31*, 1991–1999.

Fort, A.G., Murray, J.W., Dandachi, N., Davidson, M.W., Dermietzel, R., Wolkoff, A.W., and Spray, D.C. (2011). In vitro motility of liver connexin vesicles along microtubules utilizes kinesin motors. J. Biol. Chem. *286*, 22875–22885.

Gerhart, D.Z., Broderius, M.A., Borson, N.D., and Drewes, L.R. (1992). Neurons and microvessels express the brain glucose transporter protein GLUT3. Proc. Natl. Acad. Sci. USA *89*, 733–737.

Glater, E.E., Megeath, L.J., Stowers, R.S., and Schwarz, T.L. (2006). Axonal transport of mitochondria requires milton to recruit kinesin heavy chain and is light chain independent. J. Cell Biol. *173*, 545–557.

Hall, C.N., Klein-Flügge, M.C., Howarth, C., and Attwell, D. (2012). Oxidative phosphorylation, not glycolysis, powers presynaptic and postsynaptic mechanisms underlying brain information processing. J. Neurosci. *32*, 8940–8951.

Hart, G.W., Slawson, C., Ramirez-Correa, G., and Lagerlof, O. (2011). Cross talk between O-GlcNAcylation and phosphorylation: roles in signaling, transcription, and chronic disease. Annu. Rev. Biochem. *80*, 825–858.

Hornbeck, P.V., Kornhauser, J.M., Tkachev, S., Zhang, B., Skrzypek, E., Murray, B., Latham, V., and Sullivan, M. (2012). PhosphoSitePlus: a comprehensive resource for investigating the structure and function of experimentally determined post-translational modifications in man and mouse. Nucleic Acids Res. *40* (Database issue), D261–D270.

Hou, B.H., Takanaga, H., Grossmann, G., Chen, L.Q., Qu, X.Q., Jones, A.M., Lalonde, S., Schweissgut, O., Wiechert, W., and Frommer, W.B. (2011). Optical sensors for monitoring dynamic changes of intracellular metabolite levels in mammalian cells. Nat. Protoc. *6*, 1818–1833.

Huang, C.W., Huang, C.C., Cheng, J.T., Tsai, J.J., and Wu, S.N. (2007). Glucose and hippocampal neuronal excitability: role of ATP-sensitive potassium channels. J. Neurosci. Res. *85*, 1468–1477.

Iyer, S.P., and Hart, G.W. (2003). Roles of the tetratricopeptide repeat domain in O-GlcNAc transferase targeting and protein substrate specificity. J. Biol. Chem. *278*, 24608–24616.

Iyer, S.P., Akimoto, Y., and Hart, G.W. (2003). Identification and cloning of a novel family of coiled-coil domain proteins that interact with O-GlcNAc transferase. J. Biol. Chem. *278*, 5399–5409.

Ji, S., Kang, J.G., Park, S.Y., Lee, J., Oh, Y.J., and Cho, J.W. (2011). O-GlcNAcylation of tubulin inhibits its polymerization. Amino Acids *40*, 809–818.

Kang, J.S., Tian, J.H., Pan, P.Y., Zald, P., Li, C., Deng, C., and Sheng, Z.H. (2008). Docking of axonal mitochondria by syntaphilin controls their mobility and affects short-term facilitation. Cell *132*, 137–148.

Khidekel, N., Ficarro, S.B., Clark, P.M., Bryan, M.C., Swaney, D.L., Rexach, J.E., Sun, Y.E., Coon, J.J., Peters, E.C., and Hsieh-Wilson, L.C. (2007). Probing the dynamics of O-GlcNAc glycosylation in the brain using quantitative proteomics. Nat. Chem. Biol. *3*, 339–348.

Lazarus, M.B., Nam, Y., Jiang, J., Sliz, P., and Walker, S. (2011). Structure of human O-GlcNAc transferase and its complex with a peptide substrate. Nature *469*, 564–567.

Li, Y., Lim, S., Hoffman, D., Aspenstrom, P., Federoff, H.J., and Rempe, D.A. (2009). HUMMR, a hypoxia- and HIF-1alpha-inducible protein, alters mitochondrial distribution and transport. J. Cell Biol. *185*, 1065–1081.

Liesa, M., and Shirihai, O.S. (2013). Mitochondrial dynamics in the regulation of nutrient utilization and energy expenditure. Cell Metab. *17*, 491–506.

Liu, X., and Hajnóczky, G. (2011). Altered fusion dynamics underlie unique morphological changes in mitochondria during hypoxia-reoxygenation stress. Cell Death Differ. *18*, 1561–1572.

López-Doménech, G., Serrat, R., Mirra, S., D'Aniello, S., Somorjai, I., Abad, A., Vitureira, N., García-Arumí, E., Alonso, M.T., Rodriguez-Prados, M., et al. (2012). The Eutherian Armcx genes regulate mitochondrial trafficking in neurons and interact with Miro and Trak2. Nat. Commun. *3*, 814.

Love, D.C., and Hanover, J.A. (2005). The hexosamine signaling pathway: deciphering the "O-GlcNAc code". Sci. STKE *2005*, re13.

Macaskill, A.F., Rinholm, J.E., Twelvetrees, A.E., Arancibia-Carcamo, I.L., Muir, J., Fransson, A., Aspenstrom, P., Attwell, D., and Kittler, J.T. (2009). Miro1 is a calcium sensor for glutamate receptor-dependent localization of mitochondria at synapses. Neuron *61*, 541–555.

Matthews, J.A., Belof, J.L., Acevedo-Duncan, M., and Potter, R.L. (2007). Glucosamine-induced increase in Akt phosphorylation corresponds to increased endoplasmic reticulum stress in astroglial cells. Mol. Cell. Biochem. *298*, 109–123.

Nie, D., and Sahin, M. (2012). A genetic model to dissect the role of Tsc-mTORC1 in neuronal cultures. Methods Mol. Biol. *821*, 393–405.

Nunnari, J., and Suomalainen, A. (2012). Mitochondria: in sickness and in health. Cell *148*, 1145–1159.

Park, J.H., Schroeder, A.J., Helfrich-Förster, C., Jackson, F.R., and Ewer, J. (2003). Targeted ablation of CCAP neuropeptide-containing neurons of Drosophila causes specific defects in execution and circadian timing of ecdysis behavior. Development *130*, 2645–2656.

Pathak, D., Sepp, K.J., and Hollenbeck, P.J. (2010). Evidence that myosin activity opposes microtubule-based axonal transport of mitochondria. J. Neurosci. *30*, 8984–8992.

Peppiatt, C., and Attwell, D. (2004). Neurobiology: feeding the brain. Nature *431*, 137–138.

Pilling, A.D., Horiuchi, D., Lively, C.M., and Saxton, W.M. (2006). Kinesin-1 and Dynein are the primary motors for fast transport of mitochondria in Drosophila motor axons. Mol. Biol. Cell *17*, 2057–2068.

Ruan, H.B., Han, X., Li, M.D., Singh, J.P., Qian, K., Azarhoush, S., Zhao, L., Bennett, A.M., Samuel, V.T., Wu, J., et al. (2012). O-GlcNAc transferase/host cell factor C1 complex regulates gluconeogenesis by modulating PGC-1α stability. Cell Metab. *16*, 226–237.

Ruan, H.B., Singh, J.P., Li, M.D., Wu, J., and Yang, X. (2013). Cracking the O-GlcNAc code in metabolism. Trends Endocrinol. Metab. *24*, 301–309.

Saxton, W.M., and Hollenbeck, P.J. (2012). The axonal transport of mitochondria. J. Cell Sci. *125*, 2095–2104.

Schneider, C.A., Rasband, W.S., and Eliceiri, K.W. (2012). NIH Image to ImageJ: 25 years of image analysis. Nat. Methods *9*, 671–675.

Schuldiner, O., Berdnik, D., Levy, J.M., Wu, J.S., Luginbuhl, D., Gontang, A.C., and Luo, L. (2008). piggyBac-based mosaic screen identifies a postmitotic function for cohesin in regulating developmental axon pruning. Dev. Cell *14*, 227–238.

Schwarz, T.L. (2013). Mitochondrial trafficking in neurons. Cold Spring Harb. Perspect. Biol. *5*, a011304.

Silver, I.A., and Erecińska, M. (1994). Extracellular glucose concentration in mammalian brain: continuous monitoring of changes during increased

neuronal activity and upon limitation in oxygen supply in normo-, hypo-, and hyperglycemic animals. J. Neurosci. *14*, 5068–5076.

Stowers, R.S., Megeath, L.J., Górska-Andrzejak, J., Meinertzhagen, I.A., and Schwarz, T.L. (2002). Axonal transport of mitochondria to synapses depends on milton, a novel Drosophila protein. Neuron *36*, 1063–1077.

Tallent, M.K., Varghis, N., Skorobogatko, Y., Hernandez-Cuebas, L., Whelan, K., Vocadlo, D.J., and Vosseller, K. (2009). In vivo modulation of O-GlcNAc levels regulates hippocampal synaptic plasticity through interplay with phosphorylation. J. Biol. Chem. *284*, 174–181.

Trinidad, J.C., Barkan, D.T., Gulledge, B.F., Thalhammer, A., Sali, A., Schoepfer, R., and Burlingame, A.L. (2012). Global identification and characterization of both O-GlcNAcylation and phosphorylation at the murine synapse. Mol. Cell. Proteomics *11*, 215–229.

van Spronsen, M., Mikhaylova, M., Lipka, J., Schlager, M.A., van den Heuvel, D.J., Kuijpers, M., Wulf, P.S., Keijzer, N., Demmers, J., Kapitein, L.C., et al. (2013). TRAK/Milton motor-adaptor proteins steer mitochondrial trafficking to axons and dendrites. Neuron *77*, 485–502.

Visscher, K., Schnitzer, M.J., and Block, S.M. (1999). Single kinesin molecules studied with a molecular force clamp. Nature *400*, 184–189.

Wang, X., and Schwarz, T.L. (2009a). Imaging axonal transport of mitochondria. Methods Enzymol. *457*, 319–333.

Wang, X., and Schwarz, T.L. (2009b). The mechanism of Ca2+ -dependent regulation of kinesin-mediated mitochondrial motility. Cell *136*, 163–174.

Wang, X., Winter, D., Ashrafi, G., Schlehe, J., Wong, Y.L., Selkoe, D., Rice, S., Steen, J., LaVoie, M.J., and Schwarz, T.L. (2011). PINK1 and Parkin target Miro for phosphorylation and degradation to arrest mitochondrial motility. Cell *147*, 893–906.

Weisová, P., Concannon, C.G., Devocelle, M., Prehn, J.H., and Ward, M.W. (2009). Regulation of glucose transporter 3 surface expression by the AMP-activated protein kinase mediates tolerance to glutamate excitation in neurons. J. Neurosci. *29*, 2997–3008.

Yi, W., Clark, P.M., Mason, D.E., Keenan, M.C., Hill, C., Goddard, W.A., 3rd, Peters, E.C., Driggers, E.M., and Hsieh-Wilson, L.C. (2012). Phosphofructokinase 1 glycosylation regulates cell growth and metabolism. Science *337*, 975–980.

Zala, D., Hinckelmann, M.V., Yu, H., Lyra da Cunha, M.M., Liot, G., Cordelières, F.P., Marco, S., and Saudou, F. (2013). Vesicular glycolysis provides on-board energy for fast axonal transport. Cell *152*, 479–491.